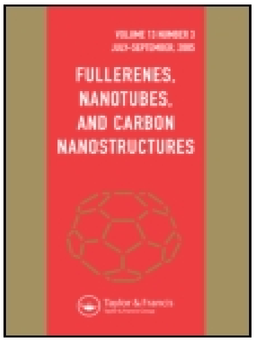


Fullerenes, Nanotubes and Carbon Nanostructures

ISSN: 1536-383X (Print) 1536-4046 (Online) Journal homepage: http://www.tandfonline.com/loi/lfnn20

# Synthesis and characterization of Cu-doped polymeric carbon nitride

Roberto C. Dante, Francisco M. Sánchez-Arévalo, Pedro Chamorro-Posada, José Vázquez-Cabo, Lazaro Huerta, Luis Lartundo-Rojas, Jaime Santoyo-Salazar, Omar Solorza-Feria, Antonio Diaz-Barrios, Tamara Zoltan, Franklin Vargas, Tatiana Valenzuela, Florinella Muñoz-Bisesti & Francisco Javier Quiroz-Chávez

**To cite this article:** Roberto C. Dante, Francisco M. Sánchez-Arévalo, Pedro Chamorro-Posada, José Vázquez-Cabo, Lazaro Huerta, Luis Lartundo-Rojas, Jaime Santoyo-Salazar, Omar Solorza-Feria, Antonio Diaz-Barrios, Tamara Zoltan, Franklin Vargas, Tatiana Valenzuela, Florinella Muñoz-Bisesti & Francisco Javier Quiroz-Chávez (2016) Synthesis and characterization of Cu-doped polymeric carbon nitride, Fullerenes, Nanotubes and Carbon Nanostructures, 24:3, 171-180, DOI: 10.1080/1536383X.2015.1124864

**To link to this article:** http://dx.doi.org/10.1080/1536383X.2015.1124864

FULLERENES, NANOTUBES AND CARBON NANOSTRUCTURES
2016, VOL. 24, NO. 3, 171–180
http://dx.doi.org/10.1080/1536383X.2015.1124864

# Synthesis and characterization of Cu-doped polymeric carbon nitride

Roberto C. Dante[a], Francisco M. Sánchez-Arévalo[b], Pedro Chamorro-Posada[c], José Vázquez-Cabo[d], Lazaro Huerta[b], Luis Lartundo-Rojas[e], Jaime Santoyo-Salazar[f], Omar Solorza-Feria[g], Antonio Diaz-Barrios[h], Tamara Zoltan[i], Franklin Vargas[i], Tatiana Valenzuela[j], Florinella Muñoz-Bisesti[j], and Francisco Javier Quiroz-Chávez[k]

[a]Facultad de Mecánica, Escuela Politécnica Nacional (EPN), Ladrón de Guevara E11–253, Quito, Ecuador; [b]Instituto de Investigaciones en Materiales, Universidad Nacional Autónoma de México, Apdo. Postal 70-360, Cd. Universitaria, México D.F., Mexico; [c]Dpto. de Teoría de la Señal y Comunicaciones e IT, Universidad de Valladolid, ETSI Telecomunicación, Paseo Belén 15, Valladolid, Spain; [d]Dpto. de Teoría de la Señal y Comunicaciones, Universidad de Vigo, ETSI Telecomunicación, Lagoas Marcosende s/n, Vigo, Spain; [e]Instituto Politécnico Nacional, Centro de Nanociencias y Micro y Nanotecnologías de Nanociencias, UPALM, Zacatenco México-D.F., México; [f]Departamento de Física, Centro de Investigación y de Estudios, Avanzados del Instituto Politécnico Nacional, CINVESTAV-IPN, Apdo. Postal 14-740, México D.F., México; [g]Departamento de Química, Centro de Investigación y de Estudios Avanzados del Instituto Politécnico Nacional (CINVESTAV), Av. IPN 2508, Col. San Pedro Zacatenco, Apdo. Postal 14-740, México D.F., México; [h]Gerencia de Educación Ciencia y Tecnología, Yachay EP, Amazonas N26-146 y la Niña, Zona Postal 170143, Quito, Ecuador; [i]Centro de Química, Laboratorio de Fotoquímica, Instituto Venezolano de Investigaciones Científicas (IVIC), Carretera Panamericana Km 11, San Antonio de los Altos, Edo. Miranda, Venezuela; [j]Departamento de Ciencias Nucleares, Escuela Politécnica Nacional (EPN), Ladrón de Guevara, Quito, Ecuador; [k]Centro de Investigaciones Aplicadas a Polímeros (CIAP), Escuela Politécnica Nacional (EPN), Ladrón de Guevara, Quito, Ecuador

**ABSTRACT**

Polymeric carbon nitride doped with copper through a solid-state reaction was characterized by several techniques, among them are UV-visible spectroscopy, infrared spectroscopy, X-ray photoelectron spectroscopy, etc. The material is a semiconductor with a wide band gap of 2.74 eV. Sites of both Cu(I) and Cu(II) were detected, apparently only coordinated by the polymer. The material comprises crumpled nanosheets, and is substantially an amorphous layered material with a prevalent 2D structure with low inter-planar interactions, as shown by X-ray diffractometry and TeraHertz spectroscopy. Photo-oxidation of benzyl alcohol was used to probe the active sites of the material, comparing them with the non-doped material. The higher activity and selectivity toward salicylic alcohol of the non-doped material can be due to both a more localized electron transfer and a longer lifetime of the hole–electron pair. Cu-CN favored the oxidation of hydroxymethyl group. Therefore, the presence of copper can favor different reaction pathways with respect to the non-doped material.

**ARTICLE HISTORY**
Received 19 October 2015
Accepted 23 November 2015

**KEYWORDS**
carbon nitride; nanosheets; THz spectroscopy; organic semiconductors

## Introduction

Polymeric carbon nitride, apart from its applications as the precursor for the synthesis of super hard carbon nitride phases (1–10), has also been investigated for a number of other applications (11–15). For example, combining chemical sensitivity with optical and semiconductor properties, polymeric carbon nitride becomes an interesting candidate for a wide field of sensors (16–20). However, most expectations are related to its potential as a photo-catalyst due to its semiconductor properties coupled with the ability to host co-catalysts. However, for many reactions, polymeric carbon nitride exhibits considerable catalytic properties without any metallic co-catalyst (15). In spite of these results, in order to increase either conversion or selectivity, it has been doped with several transition metals such as Pt, Fe, Cu, etc. Moreover, polymeric carbon nitride has been used as a photo-catalyst to produce hydrogen by splitting water (21), in photo-ionization of free radical polymerization, and in Friedel–Crafts reactions, to selectively oxidize aromatic compounds such as benzyl alcohol to benzaldehyde and to hydroxylate aromatic rings (22). Mesoporous carbon nitride impregnated by solutions of either $ZnCl_2$, $FeCl_3$, $CoCl_2$, $NiCl_2$, or $MgCl_2$ favors the cyclo-addition of $CO_2$ to propylene oxide. In this case, carbon nitride seems to work as a support to absorb $CO_2$, where the most catalytic activity is due the metal sites (23). This semiconductor material is often coupled with a co-catalyst to either improve yield or increase selectivity. The structure of polymeric carbon nitride can coordinate metallic ions, which in turn can coordinate reagent molecules. The basic mechanism exploits the optical wide band gap to excite electrons under proper lighting, which are transferred through metallic co-catalyst to the reagents to form very reactive radicals facilitating redox reactions.

Sridharan et al. (24) used metal nitrates, such as Fe, Ni, and Co nitrates, to form oxides embedded or grafted into a carbon nitride matrix. They provided an extraordinary broad absorption in the visible spectrum with band gaps estimated around 1.7 eV, due to the elevated concentration of metal oxide, against the standard 2.8–3.0 eV of pure carbon nitride. They were very efficient toward the degradation of Rhodamine B dye, and their magnetic properties make them easily recoverable and suitable

**CONTACT** Roberto C. Dante rcdante@yahoo.com 2D to 3D srls, R&D, Via Santuario 27B Moretta, 12033, Italy.
Color versions of one or more of the figures in the article can be found online at www.tandfonline.com/lfnn.
Supplemental materials data for this article can be accessed on the publisher's website.

to be used as magnetically controlled optical limiters (24). The catalytic activity of carbon nitride toward transesterification of keto esters (25) was also reported. Dadashi-Silab et al. (26) used Cu(II) chloride with pentamethyldyethylenetriamine (PMDETA), photo-reduced to Cu(I) with the aid of mesoporous carbon nitride, to a Cu(I)-catalyzed azide–alkyne cycloaddition (CuAAC), an example of click reaction, with a relevant contribution of light intensity (UV or sunlight).

Our research report presents the characterization of our Cu-doped polymer carbon nitride to understand better how copper is interacting with the material structure, as well as the effect of copper on the main electronic properties of this multipurpose material. Our synthesis pathway of polymeric carbon nitride was developed by Dante et al. (27, 29–32). The polycondensation reaction was carried out starting directly from melamine cyanurate – the adduct of melamine and cyanuric acid – which crystallizes in layers as graphite (16) and lead to crumpled nanosheets of polymeric carbon nitride. Moreover, copper has been added directly into the reagent blend as Cu(II) sulfate in a similar way as in the case of the nitrates used by Sridharan et al. (24) but with a lower concentration in order to favor its incorporation during the reaction into the polymeric structure without altering too much both structure and main electronic characteristics. The material has been characterized with several techniques such as infrared spectroscopy, UV-Vis spectroscopy, X-ray photoelectron spectroscopy, transmission microscopy, scanning electron microscopy, etc. In order to understand better the structure and nature of the material doped with copper, benzyl alcohol was used as a probe to highlight differences in the photo-catalytic oxidation behavior of the copper-doped material and the non-doped one. This idea is based on the recently discovered photo-catalytic behavior of polymeric carbon nitride, which seems to strongly depend on the material structure, as found by Zhao et al. (33) apart from the band gap considerations. For example, Zhao et al. (33) attributed the excellent activity of their carbon nitride material to the co-contribution of enlarged surface areas, strengthened electron–hole separation efficiency, enhanced electrons reduction capability, and prolonged charge carriers lifetime. Wang et al. (34) also underlined the importance of carriers' lifetime. Moreover, Zhao et al. (35) emphasized the control of the hole–electron recombination in a recent review and showed the great variety of catalysts that can be obtained by engineering the electronic properties of carbon nitride through heterojunctions and heterostructures. Therefore, the presence of copper can lead to different catalytic behaviors that can favor different reaction pathways with respect to the non-doped material. This could be due to both different electronic properties and coordination effects.

## Materials, and experimental and theoretical methods

### Materials

The reagent, melamine cyanurate, was supplied by Nachmann S.r.l. (Italy) with a purity higher than 99%. Melamine cyanurate was manually milled in an agate mortar for about 5 min; subsequently, the sample was treated with 0.1 M Cu(II) sulfate solution overnight and dried at 110°C for 6 h to favor dispersion of copper within melamine cyanurate. The sulfate-treated sample of about 4 g was placed in a ceramic crucible, and thermally treated at 600°C. The photo-catalytic behavior of the copper-doped material (Cu-CN) was compared with standard polymeric carbon nitride produced by pyrolysis of melamine cyanurate, whose synthesis method and characteristics were widely discussed in previous reports (27–32).

### Structural characterization

#### X-ray diffraction measurements

The X-ray diffraction patterns were obtained by a powder diffractometer Rigaku ULTIMA-IV with Cu K$\alpha$ radiation. Glass capillaries were used for sample mounting. The samples were ground in an agate mortar and sifted. The measurements always lasted for 1 h, and crystalline silicon was used as a standard.

#### FT-IR spectroscopy

The infrared spectra were obtained by means of a Thermo Nicolet 380 Fourier transform–infrared (FT-IR) sepectrometer (Nicolet, USA). KBr tablets of the specimens were used to identify chemical functional groups.

#### TEM and SEM characterization

Scanning electron microscope (SEM) JEOL 6300 (JEOL, Japan) was used to study the morphology and composition of samples; the last one by means energy-dispersive X-ray spectroscopy (EDS) Bruker probe (127 eV). In addition, to explore in more detail the structure of polymeric carbon nitride, transmission electron microscopy (TEM) was performed with a JEOL JEM-FS2010 HRP (JEOL, Japan).

### Thermal analysis

The thermal stability and decomposition rate of polymeric carbon nitride from melamine cyanurate was evaluated by thermogravimetric analysis using an STD Q600 thermobalance (TA Instruments, USA) with a nitrogen mass flow rate of 25 mL/min and a temperature increment rate of 10°C/min.

#### UV-Vis spectroscopy

UV-Vis diffuse reflectance spectra were measured using a Perkin Elmer Lambda 35 UV-Vis spectrophotometer. A Spectralon® blank was used as reference. The reflectance data were transformed to absorbance data by applying the Kubelka–Munk method as follows:

$$F(R) = \frac{(1-R)^2}{2R}, \quad (1)$$

where $R$ is the reflectance, and $F(R)$ is the Kubelka–Munk (K-M) function. The K-M function was plotted as a function of the energy ($E = hc/\lambda$), and the band gap value was calculated through the inflection point of this curve. The abscissa of this point is directly associated with the band-gap value (36).

### *TeraHertz (THz)–Time Domain Spectroscopy (TDS) Measurements*

A Menlo Tera K15 spectrometer was used for the THz-TDS analysis. The system is based on a 1560-nm fiber laser that generates 90-fs pulses at a repetition rate of 100 MHz. This provides a compact fiber-coupled setup. The system was operated in a nitrogen-rich atmosphere to avoid the signature of water absorption in recorded samples. Ten samples and ten reference measurements were performed in each case to reduce noise in the measurements.

The material parameters in the spectral range of interest were calculated from the time domain photocurrent traces measured with the spectrometer. These time domain waveforms depend not only on the material data but also on the width of the pellets due to the contributions from multiple reflections at the pellet–air interfaces. Signal processing techniques similar to those described by Duvillaret et al. (37) were employed to obtain the THz spectra of materials.

### *X-ray photoelectron spectroscopy*

X-ray photoelectron spectra were collected using a K-Alpha spectrometer from Thermo Scientific with monochromatic AlKa (1486 eV) radiation with an energy resolution of 0.5 eV. Wide and narrow spectra, using an X-ray spot size of 400 $\mu m^2$, were collected at 160 and 60 eV pass energy analyzer respectively. The recorded spectra were fitted through a Gaussian–Lorentzian combination based on an Offset Shirley background type.

### *Quantum chemistry computations*

The semiempirical quantum chemistry computations were performed with the PM6 method (38) using parallel implementation for multi-threaded shared-memory CPUs and massively parallel GPU acceleration (39) of MOPAC2012 (40) software package. A Fedora Linux server with a 12-core Intel Xeon processor and a NVIDIA Tesla K20 GPU was used for computations.

More details on the following photo-catalysis tests, procedure, and results are provided in Supplemental Materials section.

### *Determination of hydroxyl radical generation by fluorescence in heterogeneous phase*

The hydroxyl radicals produced from photo-catalysts were detected and quantified via fluorescence; for this, hydroxylation reaction of terephthalic acid (41, 42) was employed in heterogeneous phase.

### *Determination of singlet oxygen in heterogeneous phase*

Singlet oxygen determinations were carried out employing a modification of histidine test (43) that was measured in heterogeneous phase.

### *Photo-catalytic oxidation of benzylic alcohol*

The photo-oxidation of benzyl alcohol was conducted in the presence of a source of reactive oxygen. The first route was based on hydrogen peroxide 30% v/v, which was used with an excess of 10 times to respect benzyl alcohol, while the second one consisted of bubbling pure oxygen, with a flow rate of 0.4 l $min^{-1}$.

## Results and discussion

### *Infrared spectroscopy*

The FT-IR spectra of Cu-CN is shown in Figure 1 and compared with that of standard polymeric carbon nitride. The bands between 3500 $cm^{-1}$ and 3000 $cm^{-1}$ are due to NH stretching, whereas the bands at 3260, 3160, and 3070 $cm^{-1}$ are due to NH interacting via hydrogen bond. It is noteworthy to point out that the NH stretching bands are much weaker for Cu-CN than those of CN, indicating that cross-linking advanced even consuming more NH bonds. The band around 1622 $cm^{-1}$ is assigned to the conjugated CN stretching, and the other bands between 1580 $cm^{-1}$ and 1458 $cm^{-1}$ belong to the stretching modes of tri-s-triazine ring. The peak at 1392 $cm^{-1}$ may belong to the C-N stretching of the tertiary bridging nitrogen in the mid of the tri-s-triazine ring, the others between 1330 $cm^{-1}$ and 1200 $cm^{-1}$ belong to secondary bridging nitrogen (all associated with the four bands of NH stretching) (44) and primary amines. It should be noted that the shoulder around 1330 $cm^{-1}$ is weaker in Cu-CN corresponding to the much weaker absorption around 3470 $cm^{-1}$. The peak at 892 $cm^{-1}$ can be associated with a mode of cross-linked heptazine deformation. The sharp peak at 807 $cm^{-1}$ can be assigned to a tri-s-triazine ring mode of bending (26, 45). The spectrum of Cu-CN did not show any evident effect of copper presence and is very similar to that of CN.

### *Thermal gravimetric analysis (TGA)*

The TGA curve (see Figure 2) shows the behavior typical of a stable polymeric carbon nitride with the onset of around 550°C (46). The main thermal characteristic of CN and Cu-CN is almost the full endothermic decomposition of polymer, which makes it suitable for flame retardant

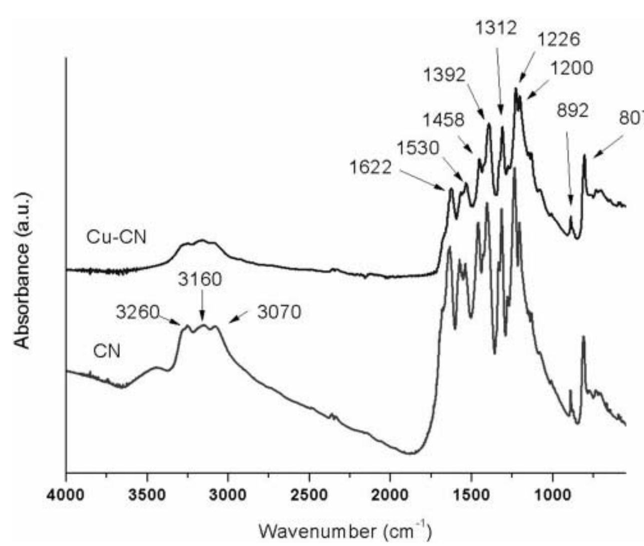


Figure 1. FT-IR spectra of Cu-CN and CN.

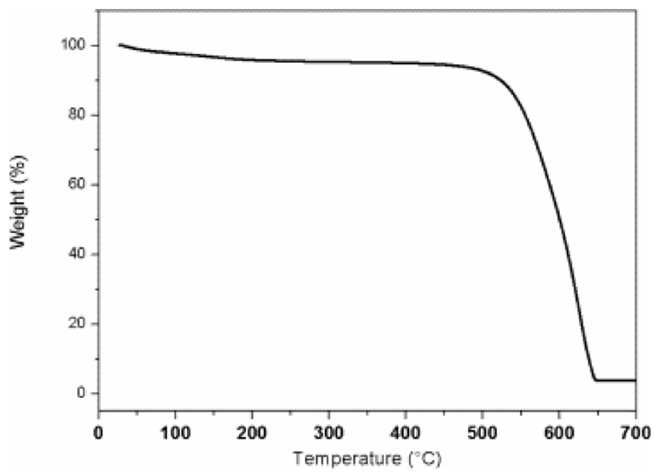


**Figure 2.** TGA curve of Cu-CN.

applications. No traces are found of other weight loss related to other compounds. The residue of 3 wt% can be attributed to copper compounds.

### Morphology of Cu-CN: SEM and TEM Analysis

The SEM image in Figure 3(a) shows the presence of platelet particles with size below 1 $\mu$m (32).

In addition, TEM revealed that the platelets observed by SEM comprise nanoflakes showing crumpled structures (see Figure 3(b)), which is in agreement with the structures reported previously in literature (27–32).

The energy-dispersive X-ray analysis showed that the average of atomic composition percentage was as follows: $N_2$ = 58 ± 2%, C = 36 ± 1%, $O_2$ = 5 ± 1%, and Cu = 0.27 ± 0.1%. Note that the missing 0.73% was identified as a combination of impurities of Si, Zn, and Na. The analysis results of the five tested regions are reported in Figure 4.

### UV-Vis

The UV-Vis spectra in Figure 5 shows where the band gap value for CN-Cu was estimated using the K-M absorbance function, and its gap energy was 2.74 eV; this value corresponds to a semiconductor n-type polymer network, as is previously reported for similar materials (30). This value is below those of non-doped materials produced with similar methods, which usually exhibit band gap between 2.8 eV and 3.3 eV (30). Probably copper doping did not cause a considerable band change because it is not directly bonded to the polymer but only coordinated by its polar groups.

### X-ray photoelectron spectroscopy

In order to identify, estimate the surface elemental composition, and establish in more detail the chemical species of the polymeric carbon nitride samples, three measurements at different points onto the surface of samples were carried out by XPS analysis. Similarly, C1s peak at 284.5 eV was employed as an internal standard to detect and compensate errors related with charge shift. It should be noted that the collected high-resolution XPS core lever spectra correspond to an average of the three measurements that were made at different points of the sample. The XPS survey scan of the sample showed the presence of C1s, N1s, O1s, and Cu2p, as depicted in Figure 6, and confirmed the doping of carbon nitride with copper.

In order to understand the role of functional groups and their chemical state, C1s, N1s, and Cu2p core level electron photoemission were measured (Figures 7(a)–(c)). From the adjustment of regions of C1s and N1s, the presence of the following bonds C-C, CCuN, C-CH2, C-N, and C=O was confirmed. These spectra and their deconvolutions are shown in Figures 8(a) and (b). In addition, their Bes' positions, and elemental and chemical species content are enlisted in Table 1.

The BEs of different chemical states of oxidation, in C1s high-resolution spectrum, which were present in the sample CN-Cu, were identified as follows; C-C, CCuN, C-CH2, C-N, C1, C2, C=O, C$\pi$ with BEs at 284.6, 285.3, 286.2, 287.2, 288.2, 288.8, 289.8, 293.8 ± 0.2 eV, respectively, where C1 and C2

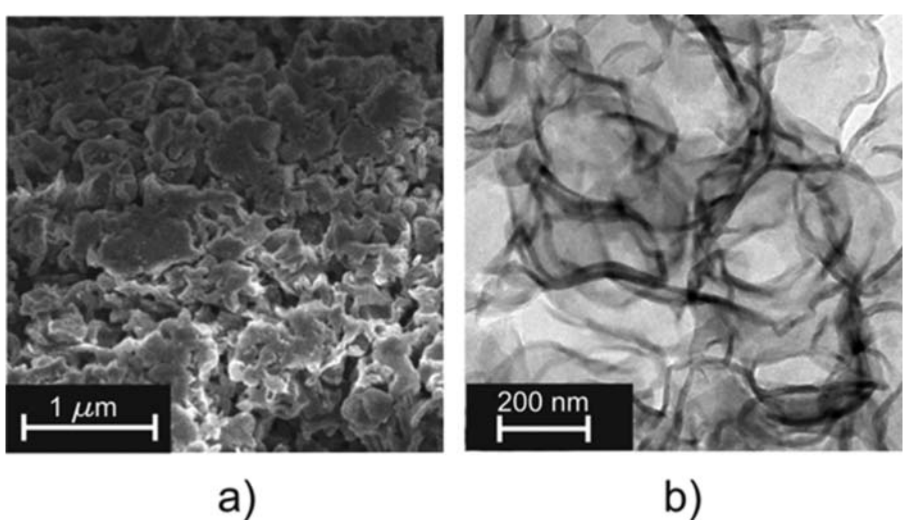


**Figure 3.** Morphology of CN-Cu. (a) SEM image, and (b) TEM image.

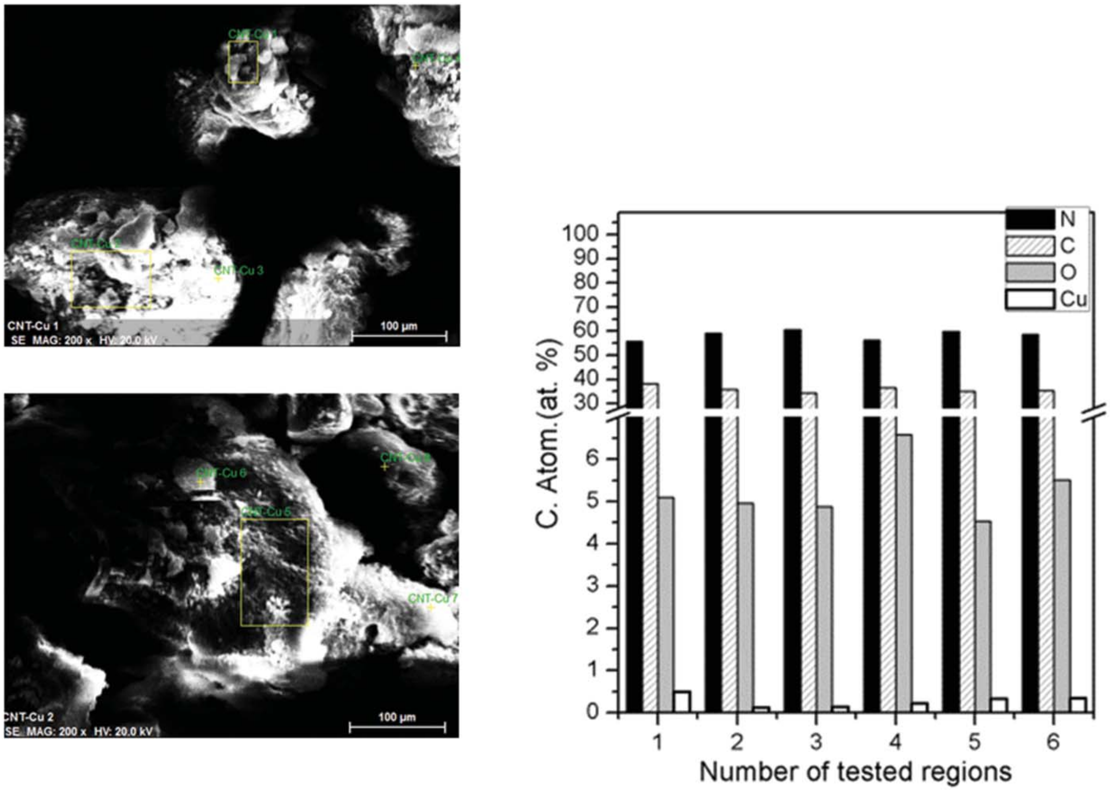


**Figure 4.** Chemical composition (in %) determined by EDS. Elements from left to right for each region: N, C, O, and Cu.

relate to the heptazine ring, and C$\pi$ denotes the delocalized electrons, due to $\pi \rightarrow \pi^*$ (31, 42–44). The contributions of nitrogen into the polymeric carbon nitride structure also were characterized by peak fitting N1s region. The peaks can be identified as CCuN, N1 (pyridine-like N, C–N=C), N2 (pyrrole-like N), N3 ("graphitic" N), N4 (primary amine or quaternary N), and N$\pi$, the delocalized electrons of N1s, associated to $\pi \rightarrow \pi^*$ transition shake-up satellites. See Figure 8 for the assignation of atoms in the polymeric carbon nitride-repeating unit according to XPS analysis.

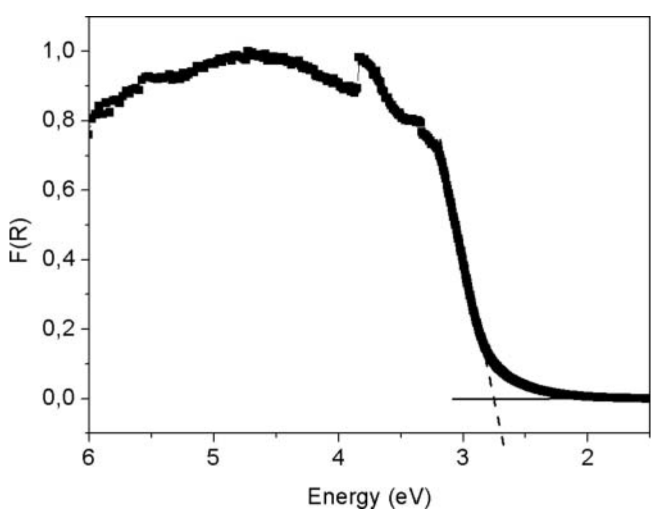


**Figure 5.** UV-Vis absorbance *F(R)* as a function of energy for Cu-CN.

The assigned BEs for the nitrogen species were 398.2, 398.7, 399.5, 400.2, 401.0, and 404.2 ± 0.2 eV respectively (47–51).

In Figure 7(c), a Cu2p core-level photoemission spectrum is shown. The broader Cu2p peak combined with difficulty to distinguish between Cu(I) and Cu(II) species, due to their photoelectron lines, do not have a large enough chemical shift to distinguish between them, and made difficult to separate and resolve accurately the CuCN signal regarding other possible minority species of Cu(I). Since the CuCN presence was upheld by other characterization techniques, Cu $2p_{3/2}$ and Cu $2p_{1/2}$ peaks were fitted with four main contributions: CuCN + Cu(I), Cu(II), $CuSO_4$, and Cu(II) shakeup satellite. Their peak positions were situated at 932.8, 933.6, 936.0 ± 0.2 eV along with 943.9 ± 0.2 eV, which were within the range of the values reported in literature (52–57). Their BEs and the estimated wt% content are also listed in Table 1. It is noted that the

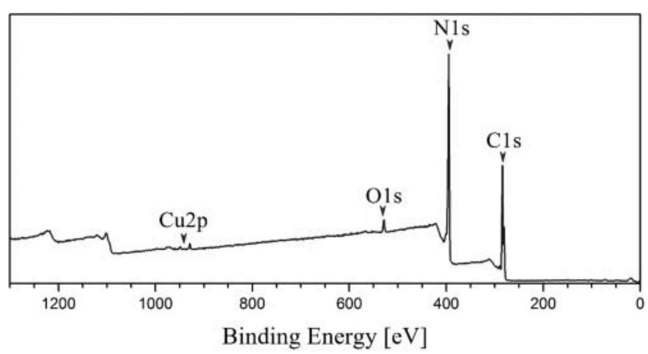


**Figure 6.** XPS analysis of CN-Cu: survey spectra showing the main peaks of CN-Cu.

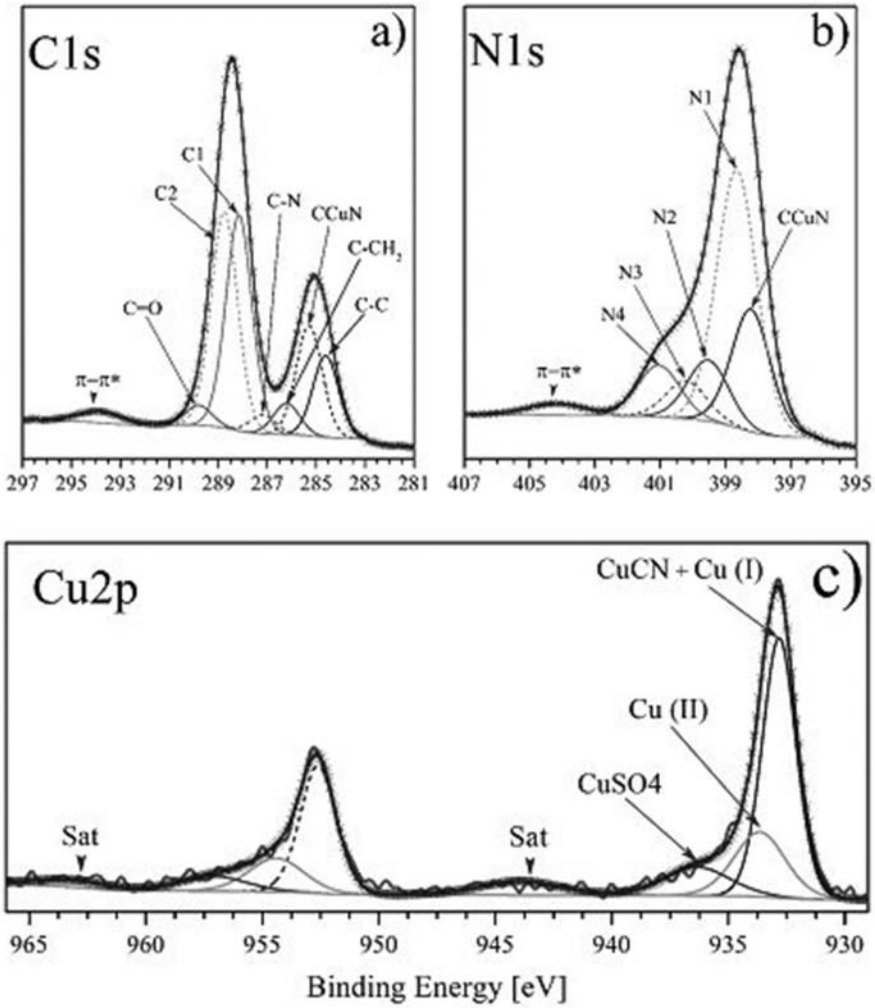


**Figure 7.** XPS analysis of Cu-CN; high-resolution spectra and deconvolution analysis for (a) C1s, (b) N1s, and (c) Cu2p.

content of CuCN is overestimated because of the inability to separate its signal from other Cu(I) chemical species.

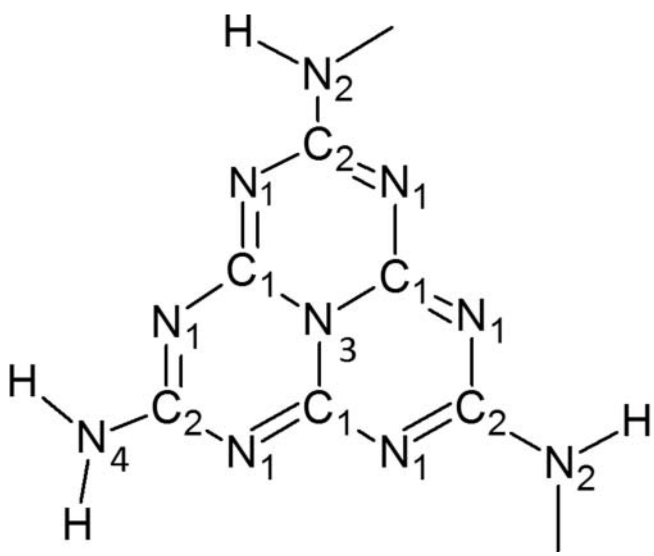

**Figure 8.** Structure of repeating polymeric carbon nitride unit with the corresponding atomic assignation according to XPS analysis.

### *THZ-TDS measurements*

The THz-TDS measurements are shown in Figure 9. The spectra of Cu-CN samples display a broad attenuation band, which is a universal feature characteristic of disordered materials (58). The observed peak shape is often the result of the combined

**Table 1.** Binding energies of C1s, N1s, and Cu2p, which are due to thespecific bonds of CN-Cu sample.

| Binding energy (±0.2 eV) | | | | | | | | |
|---|---|---|---|---|---|---|---|---|
| (Elemental wt%) | C1s (43.9) | | | | | | | |
| Sample | C-C | CCuN | C-CH2 | C-N | C1 | C2 | C=O | Cπ |
| CN-Cu | 284.6 | 285.3 | 286.2 | 287.2 | 288.2 | 288.8 | 289.8 | 293.8 |
| Wt% | 11.1 | 15.3 | 4.4 | 2.6 | 30.3 | 30.7 | 2.9 | 2.7 |
| (Elemental wt%) | N 1s (51.7) | | | | | | | |
| | CCuN | N1 | N2 | N3 | N4 | Nπ | – | – |
| CN-Cu | 398.2 | 398.7 | 399.5 | 400.2 | 401.0 | 404.2 | – | – |
| Wt% | 21.6 | 46.9 | 11.5 | 7.1 | 9.9 | 3.1 | – | – |
| (Elemental wt%) | Cu 2p3/2 (1.6) | | | | | | | |
| | CuCN + Cu(I) | Cu(II) | $CuSO_4$ | – | – | – | – | – |
| CCuN | 932.8 | 933.6 | 936.0 | – | – | – | – | – |
| Wt% | 63.0 | 23.5 | 13.5 | – | – | – | – | – |

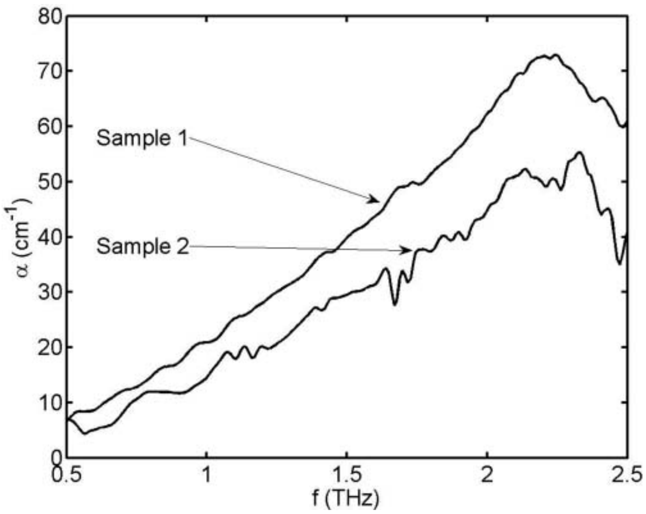


**Figure 9.** THz-TDS measurements. Sample 1 was pressed with 7 tons for 5 min, and sample 2 was pressed with 2 tons for 3 min.

effect of the reduction of dynamic range and the simultaneous increase in attenuation as frequency grows (59). Optically active vibration modes can be pertinent for the explanation of these spectra, for instance, playing a role resonance-enhanced Rayleigh scattering (60) or by their interaction with the extended far-infrared phonons (61), similar to the case of vibrational resonances in orientational glasses studied in Randeria and Sethna (62).

The universal character of this attenuation feature could be thought to be a major hindrance of this spectroscopic technique for the characterization of disordered materials. On the contrary, THz-TDS has been shown to be very effective for probing the long-range structural properties of 2D and 3D carbon and related materials (31, 60). An interpretation of the observed results grounded on theoretical investigations using semi-empirical quantum chemistry methods has been discussed in Chamorro-Posada et al. (31, 60).

Since disordered materials typically show similar spectral features, THz-TDS is particularly useful in the comparative studies of related materials (31, 60). Therefore, it is very important to keep the same conditions for the preparation of samples to avoid spurious alterations of the properties of the tested materials. We address the possible effects of pellet preparation by comparing the measurements of two samples of the same material produced under widely different conditions.

Cu-CN pellets with a diameter of 13 mm were prepared using a Graseby Specac press at CACTI (University of Vigo) for THz-TDS measurements. The results displayed in Figure 9 are consistent with a highly disordered material, possibly constituted by polymeric carbon nitride nanosheets, which have been predicted to have vibrational modes in this spectral region (31). Sample 1 was pressed with 7 tons for 5 min and sample 2 was pressed with 2 tons for 3 min. The results in Figure 9 show the same qualitative behavior but a stronger attenuation for sample 1, as expected.

## *Electrical conductivity*

For the characterization of the near-DC electrical conductivity, the pellets were placed between two copper electrodes. AC measurements were performed to avoid parasitic effects from the contacts between electrodes and pellets. These effects become negligible at sufficiently high frequency. The electrical resistance of the samples was calculated from the measured peak voltage drop and the estimation of the average power dissipated in the sample. This permits to neglect the effect of electrodes' capacitance. The conductivity was then calculated using the estimated resistance value and the pellet geometry. A very flat response was observed in all cases in the range of 100 kHz to 1 MHz, and these frequency values were used for the measurements.

Similar to the results describing the THz optical properties of the material, a dependence of electrical properties on the pressing conditions used for preparing pellets is expected. The resulting values of the conductivity are $\sigma = 8.0 \pm 0.2 \times 10^{-6}$ $Sm^{-1}$ for a sample pressed by 2 tons for 3 min and $\sigma = 3.27 \pm 0.02 \times 10^{-5}$ $Sm^{-1}$ for the sample prepared by 7 tons for 5 min. This reflects the expected relevant increase in conductivity within the same order of magnitude, for the more tightly packed pellets in accordance with the results obtained for THz attenuation. The measured values of conductivity are consistent with the semiconducting properties of the material. It is noteworthy to point out that the electric conductivity of non-doped carbon nitride is around $10^{-8}$–$10^{-9}$ $Sm^{-1}$ (63). Copper did not considerably alter the band gap but caused a considerable increment in electrical conductivity, possibly due to an increment in charge carriers. Although polymeric carbon nitride is indicated as a wide-band gap semiconductor with a certain latitude, the optical band gap only informs us about the presence of an electronic transition, which is not always related to a real semiconductor behavior (with a significant electrical conductivity, i.e. a considerable amount of charge carriers). Charge carriers are needed to sustain a significant electrical conductivity as in many other polymeric semiconductors such as polyacetylene etc. Doping has been regarded as a practical way to increase electric conductivity of polymeric semiconductors.

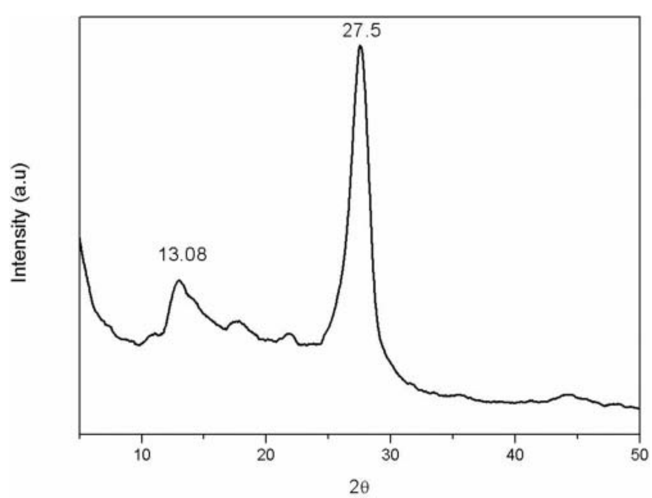


**Figure 10.** XRD pattern of Cu-CN.

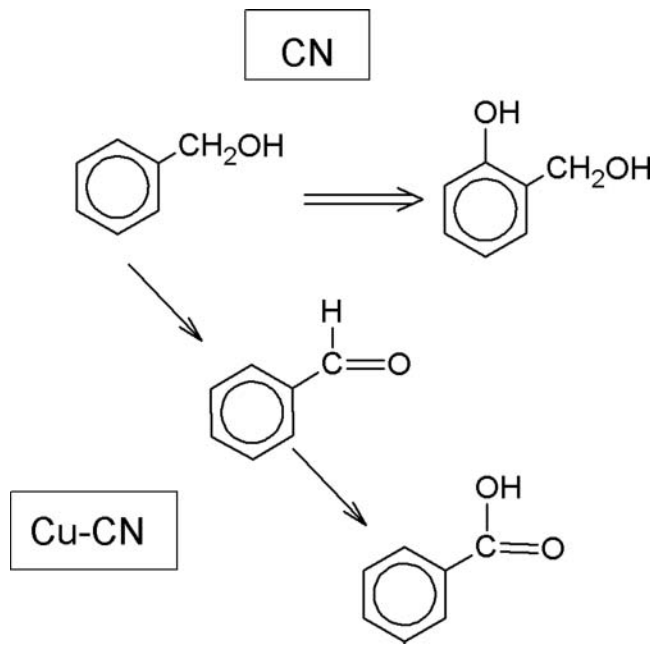


**Figure 11.** The main reaction pathways of the two photo-catalysts: CN and Cu-CN.

### *X-ray diffraction results*

The XRD pattern of CN-Cu in Figure 10 shows a material with low crystallinity and peaks characteristic of polymeric carbon nitride. In fact, it is possible to observe the characteristic broad peak around 27°; in this case, it is at 27.5°, corresponding to the 002 reflection of an essentially amorphous product with an inter-planar distance of 3.24 Å. The other characteristic peak, located at 13.08° (inter-planar distance of 6.76 Å), which is much broader and weak, belongs to an in-plane reflection. Other very weak peaks at 17.75° and 21.9° may belong to intermediates (27–32).

### *Results of photo-catalytic oxidation*

The determination of hydroxyl radical formation showed that the CN produced nearly the double of OH● radicals (105.2 $\mu$g $L^{-1}$) than Cu-CN (47.6 $\mu$g $L^{-1}$) in the set experimental conditions (data are reported in the Supplemental Materials section). This different behavior is confirmed by the benzyl alcohol photo-oxidation. In fact, CN was much more selective and active toward the hydroxylation of aromatic ring, leading to the prevalent formation of salicylic alcohol; Cu-CN, in turn, was more selective toward the oxidation of $-CH_2OH$ group leading to benzaldehyde and benzoic acid formation (64). These different pathways of reaction are displayed in Figure 11, indicating the formed products according to the selectivity of two catalysts. In the low polar CN, the benzyl alcohol aromatic ring was more exposed to electron transfer, and hence is more reactive. On the other hand, in Cu-CN, polar groups such as $-CH_2OH$ are probably coordinated by copper ions and more exposed to electron transfer. The higher reactivity of CN can be explained by a longer lifetime and higher localization of the hole–electron pair (33–35) than in Cu-CN, where a more conductive behavior can favor other dissipative ways of hole–electron recombination. Moreover, part of the electrons in Cu-CN can be absorbed by Cu(I) and Cu(II) sites in a sustained cycle of oxidization and reduction.

## Conclusions

Carbon nitride doped with copper has a band gap of 2.74 eV, below the gap of non-doped materials produced by the same methods. Sites of Cu(I) and Cu(II) were detected by X-ray photoelectron spectroscopy. The material comprises crumpled particles, and is eventually an amorphous layered material as proved by XRD and THz-TDS spectroscopy. The electric conductivity of the copper-doped material is around $10^{-5}$ $Sm^{-1}$, typical of a semiconductor and considerably higher than that of non-doped materials, which is between $10^{-8}$ $Sm^{-1}$ and $10^{-9}$ $Sm^{-1}$. The sensitivity of conductivity to the applied pressure is remarkable. Therefore, the material can be classified as a wide-band semiconductor. This difference between the copper-doped and non-doped polymeric carbon nitrides is also reflected by the photo-catalytic oxidation of benzyl alcohol with hydrogen peroxide, used as a probe to identify and compare the active sites of the two materials. Actually, the higher activity and selectivity of the non-doped carbon nitride toward salicylic alcohol formation is possibly due to the more localized electron transfer on the aromatic ring and the longer lifetime of the hole–electron pair, which allowed a more efficient transfer of electrons to reactive species. However, Cu-CN favored the oxidation of hydroxymethyl group. The more conductive Cu-CN probably offered other dissipative pathways of hole–electron pair recombination. Therefore, the presence of copper can favor different reaction pathways with respect to the non-doped material.

## Acknowledgments

The authors are grateful to Miguel Angel Canseco, Adriana Tejeda, Damaris Cabrero for their technical support for the characterization of Cu-CN. The authors are also grateful to Dr. Luis G. Rodríguez, Prometeo-Senescyt fellow at the EPN, for the measurement of the Xe-lamp spectrum.

## Funding

Roberto C. Dante and Antonio Diaz-Barrios were supported by a fellowship of the Prometeo Project issued by the Secretary of Higher Education, Science, Technology and Innovation of Ecuador (*Secretaría de Educación Superior, Ciencia, Tecnología e Innovación de la República del Ecuador, SENESCYT*).

## References

1. Cohen, M. L. (1985) Calculation of bulk moduli of diamond and zinc-blende solids. *Phys. Rev. B*, 32: 7988–7991.
2. Liu, A. Y., and Cohen, M. L. (1990) Structural properties and electronic structure of low-compressibility materials: beta -$Si_3N_4$ and hypothetical beta-$C_3N_4$. *Phys. Rev. B*, 41: 10727–10734.
3. Li, X., Zhang, J., Shen, L., Ma, Y., Lei, W., Cui, Q., and Zou, G. (2008) Preparation and characterization of graphitic carbon nitride through pyrolysis of melamine. *Appl. Phys. A.*, 94: 387–392.
4. Zhao, Y., Liu, Z., Chu, W., Song, L., Zhang, Z., Yu, D., Tian, Y., Xie, S., and Sun, L. (2008) Large-scale synthesis of nitrogen-rich carbon nitride microfibers by using graphitic carbon nitride as precursor. *Adv. Mater.*, 20: 1777–1781.

5. Dante, R. C., Martín-Gil, J., Pallavidino, L., and Geobaldo, F. (2010) Synthesis under pressure of potential precursors of CNx materials based on melamine and phenolic resins. *J. Macromol. Sci. B.*, 49: 371–382.
6. Zhang, G., Zhang, M., Ye, X., Qiu, X., Lin, S., and Wang, X. (2014) Iodine modified carbon nitride semiconductors as visible light photocatalysts for hydrogen evolution. *Adv. Mater.*, 26: 805–809.
7. Zhang, J., Sun, J., Maeda, K., Domen, K., Liu, P., Antonietti, M., Fu, X., and Wang, X. (2011) Sulfur-mediated synthesis of carbon nitride: band-gap engineering and improved functions for photocatalysis. *Energy Environ. Sci.*, 4: 675–678.
8. Zhang, Y., Bo, X., Nsabimana, A., Luhana, C., Wang, G., Wang, H., Li, M., and Guo, L. (2014) Fabrication of 2D ordered mesoporous carbon nitride and its use as electrochemical sensing platform for $H_2O_2$, nitrobenzene, and NADH detection. *Biosens. Bioelectron.*, 53: 250–256.
9. Zhang, Y., Mori, T., and Ye, J. (2012) Polymeric carbon nitrides: semiconducting properties and emerging applications in photocatalysis and photoelectrochemical energy conversion. *Sci. Adv. Mater.*, 4: 282–291.
10. Zhang, Y., Schnepp, Z., Cao, J., Ouyang, S., Li, Y., Ye, J., and Liu, S. (2013) Biopolymer-activated graphitic carbon nitride towards a sustainable photocathode. *Mater. Sci. Rep.*, 3: 2163.
11. Vinu, A., Ariga, K., Mori, T., Nakanishi, T., Hishita, S., Golberg, D., and Bando, Y. (2005) Preparation and characterization of well-ordered hexagonal mesoporous carbon nitride. *Adv. Mater.*, 17: 1648–1652.
12. Zhao, H., Lei, M., Yang, X., Jian, J., and Chen, X. (2005) Route to GaN and VN assisted by carbothermal reduction process. *J. Am. Chem. Soc.*, 127: 15722–15723.
13. Zimmerman, J. L., Williams, R., Khabashesku, V. N., and Margrave, J. L. (2001) Synthesis of spherical carbon nitride nanostructures. *Nano Lett.*, 1: 731–734.
14. Cao, C., Huang, F., Cao, C., Li, J., and Zhu, H. (2004) Synthesis of carbon nitride nanotubes via a catalytic-assembly solvothermal route. *Chem. Mater.*, 16: 5213–5215.
15. Thomas, A., Fischer, A., Goettmann, F., Antonietti, M., Müller, J.-O., Schlögl, R., and Carlsson, J. M. (2008) Graphitic carbon nitride materials: variation of structure and morphology and their use as metal-free catalysts. *J. Mater. Chem.*, 18: 4893–4908.
16. Zambov, L. M., Popov, C., Abedinov, N., Plass, M. F., Kulisch, W., Gotszalk, T., Grabiec, P., Rangelow, I. W., and Kassing, R. (2000) Gas-sensitive properties of nitrogen-rich carbon nitride films. *Adv. Mater.*, 12: 656–660.
17. Lee, S. P., Lee, J. G., and Chowdhury, S. (2008) CMOS humidity sensor system using carbon nitride film as sensing materials. *Sensors*, 8: 2662–2672.
18. Du A., Sanvito, S., Li, Z., Wang, D., Jiao, Y., Liao, T., Sun, Q., Ng, Y. H., Zhu, Z., Amal, R., and Smith, S. C. (2012) Hybrid graphene and graphitic carbon nitride nanocomposite: gap opening, electron–hole puddle, interfacial charge transfer, and enhanced visible light response. *J. Am. Chem. Soc.*, 134: 4393–4397.
19. Tian, J., Liu, Q., Asiri, A. M., Al-Youbi, A. O., and Sun, X. (2013) Ultrathin graphitic carbon nitride nanosecond: a highly efficient fluorosensor for rapid, ultrasensitive detection of Cu2+. *Anal. Chem.*, 85: 5595–5599.
20. Deifallah, M., McMillan, P. F., and Corà, F. (2008) Electronic and structural properties of two-dimensional carbon nitride graphenes. *J. Phys. Chem. C.*, 112: 5447–5453.
21. Martín-Ramos, P., Martín-Gil, J., Dante, R. C., Vaquero, F., Navarro, R. M., and Fierro, J. L. G. (2015) A simple approach to synthesize $gC_3N_4$ with high visible light photoactivity for hydrogen production. *Int. J. Hydrog. Energy*, 40: 7273–7281.
22. Gong, Y., Li, M., Li, H., and Wang, Y. (2015) Graphitic carbon nitride polymers: promising catalysts or catalyst supports for heterogeneous oxidation and hydrogenation. *Green Chem.*, 17: 715–736.
23. Xu, J., Wu, F., Jiang, Q., Shang, J., and Li, Y. (2015) Metal halides supported on mesoporous carbon nitride as efficient heterogeneous catalysts for the cycloaddition of CO2. *J. Mol. Catal. A*, 403: 77–83.
24. Sridharan, K., Kuriakose, T., Philip, R., and Park, T. J. (2014) Transition metal (Fe, Co, and Ni) oxide nanoparticles grafted graphitic carbon nitrides as efficient optical limiters and recyclable photocatalysts. *Appl. Surf. Sci.*, 308: 139–147.
25. Xu, J., Wu, F., Wu, H., Xue, B., Li, Y., and Cao, Y. (2014) Three-dimensional ordered mesoporous carbon nitride with large mesopores: synthesis and application towards base catalysis. *Micropor. Mesopor. Mater.*, 198: 223–229.
26. Dadashi-Silab, S., Kiskan, B., Antonietti, M., and Yagci, Y. (2014) Mesoporous graphitic carbon nitride as a heterogeneous catalyst for photo-induced copper(I)-catalyzed azide–alkyne cycloaddition. *RSC Adv.*, 4: 52170–52173.
27. Dante, R. C., Martín-Ramos, P., Correa-Guimaraes, A., and Martín-Gil, J. (2011) Synthesis of graphitic carbon nitride by reaction of melamine and uric acid. *Mater. Chem. Phys.*, 130: 1094–1102.
28. Heine, A., Gloe, K., Doert, T., and Gloe, K. (2008) A new supramolecular assembly formed by melamine and sulfuric acid. *Z. Anorg. Allg. Chem.*, 634: 452–456.
29. Dante, R. C., Martín-Ramos, P., Navas-Gracia, L. M., Sánchez-Arévalo, F. M., and Martín-Gil, J. (2013) Polymeric carbon nitride nanosheets. *J. Macromol. Sci. B*, 52: 623–631.
30. Dante, R. C., Martín-Ramos, P., Sánchez-Arévalo, F. M., Huerta, L., M. Bizarro, Navas-Gracia, L. M., and Martín-Gil, J. (2013) Synthesis of crumpled nanosheets of polymeric carbon nitride from melamine cyanurate. *J. Solid State Chem.*, 201: 153–163.
31. Chamorro-Posada, P., Vázquez-Cabo, J., Sánchez-Arévalo, F. M., Martín-Ramos, P., Martín-Gil, J., Navas-Gracia, L. M., and Dante, R. C. (2014) 2D to 3D transition of polymeric carbon nitride nanosheets. *J. Solid State Chem.* 219: 232–241.
32. Dante, R. C., Sánchez-Arévalo, F. M., Chamorro-Posada, P., Vázquez-Cabo, J., Huerta L., Lartundo-Rojas, L., Santoyo-Salazar, J., and Solorza-Feria, O. (2015) Supramolecular intermediates in the synthesis of polymeric carbon nitride from melamine cyanurate. *J. Solid State Chem.* 226: 170–178.
33. Zhao, Z., Sun, Y., Luo, Q., Dong, F., Li H., and Ho, W. (2015) Mass-controlled direct synthesis of graphene-like carbon nitride nanosheets with exceptional high visible light activity. Less is better. *Sci. Rep.*, 5: 14643.
34. Wang, Z., Guan, W., Sun, Y., Dong, F., Zhouc, Y., and Ho, W. (2015) Water-assisted production of honeycomb-like g-C3N4 with ultralong carrier lifetime and outstanding photocatalytic activity. *Nanoscale*. 7: 2471–2479.
35. Zhao, Z., Sun, Y., and Dong, F. (2015) Graphitic carbon nitride based nanocomposites: a review. *Nanoscale*. 7: 15–37.
36. Nowak, M., Kauch, B., and Szperlich, P. (2009) Determination of energy band gap of nanocrystalline SbSI using diffuse reflectance spectroscopy. *Rev. Sci. Instrum.*, 80: 046107.
37. Duvillaret, L., Garet, F., and Coutaz, J. L. (1996) A reliable method for extraction of material parameters in terahertz time-domain spectroscopy. *IEEE J. Select. Top. Quantum Electron.*, 2: 739–746.
38. Stewart, J. J. P., and Mo, J. (2007) Optimization of parameters for semiempirical methods V: modification of NDDO approximations and application to 70 elements. *Model*. 13: 1173–1213.
39. Maia, J. D. C., Carvalho, G. A. U., Mangueira, C. P., Santana, S. R., Cabral, L. A. F., and Rocha, G. B. (2012) GPU linear algebra lubraries and GPGPU programming for accelerating MOPAC semiempirical quantum chemistry calculations. *J. Chem. Theory Comput.* 8: 3072–3081.
40. Stewart, J. J. P. (2012) *Stewart Computational Chemistry*, Colorado Springs, CO. Accessed 16 November 2015. http://openmopac.net.
41. Ishibashi, K., Fujishima, A., Watanabe, T., and Hashimoto, K. (2000) Quantum yields of active oxidative species formed on $TiO_2$ photocatalyst. *J. Photoch. Photobio. A*, 134: 139–142.
42. Freinbichler, W., Bianchi, L., Colivicchi, M. A., Ballini, C., Tipton, K. F., Linert, W., and Corte, L. D. (2008) The detection of hydroxyl radicals in vivo. *J. Inorg. Biochem.*, 102: 1329–1333.
43. Zoltan T., Vargas F., and Izzo C. (2007) UV-Vis spectrophotometrical and analytical methodology for the determination of singlet oxygen in new antibacterials drugs. *Anal. Chem. Insights*, 2: 111–118.

44. Jürgens, B., Irran, E., Senker, J., Kroll, P., Müller, H., and Schnick, W. (2003) Melem (2,5,8-Triamino-tri-s-triazine), an important intermediate during condensation of melamine rings to graphitic carbon nitride: synthesis, structure determination by X-ray powder diffractometry, solid state NMR, and theoretical studies. *J. Am. Chem. Soc.*, 125: 10288–10300.
45. Foy, D., Demazeau, G., Florian, P., Massiot, D., Labrugère, C., and Goglio, G. (2009) Modulation of the crystallinity of hydrogenated nitrogen-rich graphitic carbon nitrides. *J. Solid State Chem.*, 182: 165–171.
46. Purdym A- P., and Callahan, J. H. (1998) Syntheses of sublimable carbon nitride materials. *Main Group Chem*., 2: 207–213.
47. Maldonado, S., Morin, S., and Stevenson, K. J. (2006) Structure, composition, and chemical reactivity of carbon nanotubes by selective nitrogen doping. *Carbon*, 44: 1429–1437.
48. Sharifi, T., Nitze, F., Barzegar, H. R., Tai, C., Mazurkiewicz, M., Malolepszy, A., Stobinski, L., and Wågberg, T. (2012) Nitrogen-doped multi-walled carbon nanotubes produced by CVD-correlating XPS and Raman spectroscopy for the study of nitrogen inclusion. *Carbon*, 50: 3535–3541.
49. Wang, X., Liu, Y., Zhu, D., Zhang, L., Ma, H., Yao, N., and Zhang, B. (2002) Controllable growth, structure, and low field emission of well-aligned CNx Nanotubes. *J. Phys. Chem. B*, 106: 2186–2190.
50. Guo-Hai, Y., Yong-Jie, L., Kumar, R. R., and Jun-Jie, Z. (2013) Nitrogen-doped graphene decorated with Pt-Au alloy nanoparticles for enhanced electrochemical activities. *J. Mater. Chem. A*, 1: 1754–1762.
51. Sharifi, T., Hu, G., Jia, X., and Wågberg, T. (2012) Formation of active sites for oxygen reduction reactions by transformation of nitrogen functionalities in nitrogen-doped carbon nanotubes. *ACS Nano*., 6: 8904–8912.
52. Klein, J. C., Proctor, A., and Hercules, D. M. (1983) X-ray excited auger intensity ratios for differentiating copper compounds. *Anal. Chem.*, 55: 2055–2059.
53. Moulder, J. F., Stickle, W. F., Sobol, P. E., and Bomben, K. D. (1995) *Handbook of X-ray Photoelectron Spectroscopy*, 2nd ed., Chastain, J. and King, R. C. (eds.), Physical Electronics: Eden Prairie, MN.
54. Bhushan, B., Fuchs, H., and Tomitori, M. (eds). (2008) *Applied Scanning Probe Methods IX: Characterization*, Springer Verlag: Berlin, Germany.
55. Li, C. W., and Kanan, M. W. (2012) $CO_2$ reduction at low overpotential on Cu electrodes resulting from the reduction of thick $Cu_2O$ films. *J. Am. Chem. Soc.*, 134: 7231–7234.
56. Alves, D. C. B., Silva, R., Voiry, D., Asefa, T., and Chhowalla, M. (2015) Copper nanoparticles stabilized by reduced graphene oxide. *Mater. Renew. Sustain. Energy*, 4: 2.
57. Naumkin, A. V., Kraut-Vass, A., and Powell, C. J. (2003) *NIST Standard Reference Database 20*, version 3.4 (web version), Washington DC: NIST. http://srdata.nist.gov/xps/.
58. Taraskin, S. N., Simdyankin, S. I., Elliot, S. R., Neilson, J. R., and Lo, T. (2006) Universal features of terahertz absorption in disordered materials. *Phys. Rev. Lett.*, 97: 055504.
59. Jepsen, P. U., and Fisher, B. M. (2005) Dynamic range in terahertz time-domain transmission and reflection spectroscopy, *Opt. Lett.* 30: 29–31.
60. Chamorro-Posada, P., Vázquez-Cabo, J., Rubiños-López, Ó., Martín-Gil, J., Hernández-Navarro, S., Martín-Ramos, P., Sánchez-Arévalo, F. M., Tamashausky, A. V., Merino-Sánchez, C., and Dante, R. C. (2016) THz TDS study of some $sp^2$ carbon materials: graphite, needle coke and graphene oxides. *Carbon*, 98: 484–490.
61. Schober, H. R., and Oligscleger, C. (1996) Low-frequency vibrations in a model glass. *Phys. Rev. B*, 53: 11469–11480.
62. Randeria, M., and Sethna, J. P. (1988) Resonant scattering and thermal transport in orientational glasses. *Phys. Rev. B*, 38: 12607–12614.
63. Zhang, Y., Mori, T., Ye, J., and Antonietti, M. (2010) Phosphorus-doped carbon nitride solid: enhanced electrical conductivity and photocurrent generation. *J. Am. Chem. Soc.*, 132: 6294–6295.
64. Markó, I. E., Giles, P. R., Tsukazaki, M., Brown, S. M., and Urch, C. J. (1996) Copper-catalyzed oxidation of alcohols to aldehydes and ketones: an efficient, aerobic alternative. *Science*, 274: 2044–2046.